F-BAR domain protein Rga7 collaborates with Cdc15 and Imp2 to ensure proper cytokinesis in fission yeast

Rebeca Martín-García*, Pedro M. Coll, and Pilar Pérez

Instituto de Biología Funcional y Genómica, Consejo Superior de Investigaciones Científicas/ Universidad de Salamanca. 37007 Salamanca, Spain.

Running title: Rga7 role in cytokinesis

Key words: Schizosaccharomyces pombe, actomyosin ring, septum, F-BAR, Rho-GAP, Cdc15, Imp2.

* Correspondence should be addressed to rebemg@usal.es

JCS Advance Online Article. Posted on 22 July 2014

SUMMARY

F-BAR domain proteins act as linkers between the cell cortex and cytoskeleton and are involved in membrane binding and bending. Rga7 is one of the seven F-BAR proteins present in fission yeast. In addition to the F-BAR domain at the N-terminal region, Rga7 possesses a Rho-GAP domain at its C-terminus. We show here that Rga7 is necessary to prevent contracting ring fragmentation and incorrect septum synthesis. Accordingly, cultures of cells lacking Rga7 contain a higher percentage of dividing cells and more frequent asymmetric or aberrant septa, which ultimately may cause cell death. Rga7 F-BAR domain is necessary for the protein localization to the division site and to the cell tips and also for the Rga7 roles in cytokinesis. In contrast, Rga7 GAP catalytic activity seems to be dispensable. Moreover, we demonstrate that Rga7 cooperates with the two F-BAR proteins Cdc15 and Imp2 to ensure proper cytokinesis. We have also detected association of Rga7 with Imp2, and its binding partners Fic1 and Pxl1. Altogether, our findings suggest that Rga7 forms part of a protein complex that coordinates late stages of cytokinesis.

INTRODUCTION

Cytokinesis is the cellular process by which two daughter cells become physically separated from each other at the end of the cell division cycle. The main machinery for cytokinesis is conserved from fungi to human, as are the key events which occur in a spatiotemporal regulated manner during this process: division plane selection, contractile actomyosin ring (CAR) assembly, contraction and disassembly, plasma membrane fusion, and cell separation (Balasubramanian et al., 2004; Barr and Gruneberg, 2007; Pollard and Wu, 2010). Unlike animal cells, fungi synthesize a division septum behind the ring as it constricts, generating cell wall material between daughter cells (Bi, 2001; Guertin et al., 2002). In the fission yeast, *Schizosaccharomyces pombe*, the division septum includes a primary septum (PS) with linear β(1,3)glucan, which is synthesized by the membrane enzyme Bgs1(Cortes et al., 2007). This PS is surrounded by a secondary septum (SS) that will form the cell wall of the new end in the daughter cells. Recent works have unveiled the importance of the presence of the main cell-wall glucans in the correct PS closure during cytokinesis (Cortes et al., 2012; Munoz et al., 2013). Moreover, it has been proposed that septum pushing force collaborates with the ring constriction (Proctor et al., 2012). Besides actin and myosin type II, a wide variety of proteins associate with the CAR and regulate the composition, dynamics, and anchoring of this structure to the plasma membrane. *S. pombe* Cdc15 is one of the first proteins observed at the forming ring (Wu et al., 2003). It is the founding member of the Pombe Cdc15 Homology (PCH) family of proteins (Lippincott and Li, 2000), which share a conserved domain architecture with an N-terminal F-BAR domain (Itoh et al., 2005; Tsujita et al., 2006) and a C-terminal SH3 domain. BAR domains are membrane-binding domains capable of promoting membrane curvature, leading either to membrane invagination or protrusion (Frost et al., 2009; Yu and Schulten, 2013). PCH proteins link the cell membrane and cytoskeleton through their F-BAR domain and recruit binding partners, through their SH3 domains, to support a variety of cellular events, including endocytosis, cytokinesis, motility and morphogenesis (Chitu and Stanley, 2007). Cdc15 has been proposed to link CAR proteins to the cell membrane at the division site (Roberts-Galbraith and Gould, 2010). Through its F-BAR domain, Cdc15 recruits the formin, Cdc12, and myosin type I (Myo1), to promote medial F-actin nucleation (Carnahan and Gould, 2003). Cdc15 also stabilizes the CAR through its SH3 domain-mediated interactions with C2-domain

protein Fic1 and paxillin, Pxl1 (Roberts-Galbraith et al., 2009). Imp2, another PCH family member, also plays a role in fission yeast cytokinesis, cooperating with Cdc15 through its SH3 domain in recruiting the proteins Fic1 and Pxl1 (Roberts-Galbraith et al., 2009) and promoting proper ring disassembly (Demeter and Sazer, 1998).

In this work we describe that the F-BAR protein Rga7 participates in fission yeast morphogenesis and cytokinesis by ensuring actomyosin ring stability as well as correct ring disassembly. Thus, *rga7*$^{+}$ deletion results in abnormal septum completion and improper cell separation. Rga7 is one of the three fission yeast Rho-GAP proteins that bears an F-BAR domain and previous studies in our group described that Rga7 is a Rho2 GAP involved in regulation of the MAPK Pmk1 signaling pathway for cell integrity (Soto et al., 2010). However, Rga7 GAP catalytic activity seems nonessential for the protein function in cytokinesis, while the F-BAR domain present at the N-terminus of the protein is necessary for correct localization and function. Furthermore, we demonstrate here that Rga7 has a cooperative role with the two F-BAR−containing proteins, Cdc15 and Imp2, in ensuring proper cytokinesis. Finally, we propose that Rga7 exerts its role in cytokinesis as part of a complex of proteins that link the actomyosin ring to the membrane to fine-tune this process.

RESULTS

Fission yeast Rga7 functions in morphogenesis, septum formation, and cell integrity

Rga7 is one of the three fission yeast Rho-GAP proteins that bears an F-BAR domain. Rga7 is a Rho2 GAP involved in regulation of the MAPK Pmk1 signaling pathway for cell integrity (Soto et al., 2010). Besides an increased Pmk1 activity, *rga7Δ* mutant strain showed a heterogeneous phenotype (**Figure 1A and 1B**): most cells were wider (on average 4.5±0.5 μm n= 50) than the wild-type cells (4±0.03 μm, n= 50) and some of them showed a swollen morphology. Cultures of *rga7Δ* cells incubated at 32ºC, presented a proportion of dead cells (on average, 13±1.2% n= 250) and cell death occurred mostly during the later steps of cytokinesis when PS is degraded (**Figure S1 A**). This cell death was only partially suppressed by the addition of 1.2M sorbitol (9±1% versus 131.2% n= 250 in the absence of sorbitol) to the culture medium suggesting that it was not only due to cell wall defects but probably to membrane defects too (**Figure S1 B**). In addition, *rga7Δ* mutant strain showed a higher percentage of cells undergoing septation (27±1.6%) compared to wild-type cells cultured at the same temperature of 32ºC (19±1.2%), and a higher percentage of cells that remained joined (paired cells) with incomplete septum degradation (23±0.9% compared to 3±0.8% in wild-type strain) (**Figure 1A and 1B**). Among the septating cells, a proportion (40±2.1%) had septum defects such as asymmetric septum formation (**Figure 1C, vii and viii**), irregular septum with a thicker area close to the center (**Figure 1A and 1C, v and vi**), and nonhomogeneous or discontinuous staining with calcofluor (**Figure 1A, inset**). There were also multiseptated cells (6.5±1.5%), whose number increased with the incubation temperature (24±1% at 36ºC) **(Figure 1A and Figure 1B**).

Transmission electron microscopy observation of *rga7*Δ cells (**Figure 1C**) showed that cells with completed septa and a thicker area towards the center had a bubble-like structure with internal material, denser to the electrons, that resembled plasma membrane **(Figure 1C, iv and vi)** and that might correspond to membrane fragments trapped between cell wall material. In addition, we confirmed the existence of asymmetric ingressing septa and septa with nonhomogeneous thickness (**Figure 1C, viii)**, which could correspond to those septa presenting an irregular calcofluor staining. 3D reconstruction analysis of several calcofluor stained septa corroborated the EM

observations (**Figure S1C and Movie 1**). All these defects suggest that Rga7 plays a role in cell morphology, cell integrity, and cytokinesis.

Rga7 is important for CAR integrity during contraction and for proper CAR disassembly, septation and cell separation

Since membrane ingression and septum formation are guided by the CAR we wondered if the CAR was defective in *rga7*Δ cells. Fluorescently tagged myosin II regulatory light chain (Rlc1-tdTomato) and syntaxin (GFP-Psy1) were used to monitor CAR morphology and plasma membrane respectively. While in wild-type cells the actomyosin ring in contraction is always positioned ahead of the ingressing plasma membrane, in some *rga7*Δ cells, CAR fragments remained behind the leading edge of the membrane suggesting that the CAR was not properly disassembled as the membrane was brought in (**Figure 2A**). Careful examination of 3-D reconstructions of the CAR, revealed that in cells lacking Rga7 cultured at 32ºC many rings, especially rings in contraction, appeared discontinuous and ring fragments were observed in different planes, on one or both sides of the initial division plane (**Figure 2B**). Cells with two or three adjacent rings were occasionally observed and the frequency of these cells increased when incubation temperature was raised to 36ºC (**Figure 2B**). These phenotype resembles that of *pxl1*Δ cells (Pinar et al., 2008) and point to an Rga7 role in maintaining CAR integrity during contraction. Genetic experiments corroborated this hypothesis since we detected synthetic lethality between *rga7*Δ and *pxl1*Δ, and negative interactions of *rga7*Δ with other mutant strains affected in CAR integrity and maintenance (**Supplementary Table S1**).

To assess whether *rga7*Δ abnormal CARs would be able to contract with the same kinetics as wild-type rings we performed time-lapse microscopy in wild-type and *rga7*Δ cells expressing Rlc1-tdTomato to visualize the contractile ring and Cut11-GFP, which labels the nuclear membrane to monitor cell cycle stage. On average, we did not find significant differences in timing for ring formation or maturation in *rga7*Δ cells (data not shown). However, Rga7 lacking cells took longer to complete CAR contraction: 27$\pm$8.9 min versus 21$\pm$ 4.7 min in wild-type cells (n=20) (**Figure 2C and 2D**). Although most *rga7*Δ cells showed a delay in CAR contraction, the timing needed to complete this process strongly varied from cell to cell as shown in the whisker box plot

(**Figure 2D**). The cells in which the ring split apart forming an adjacent ring were not taken into account for the time quantifications.

After CAR contraction, ring remnants disappeared within 9 min in wild-type cells whereas in cells lacking Rga7, rings did not disassemble properly (**Figure 2C and 2E**) and persisted for longer times (18 min. on average), extending more than 30 minutes in some cases (**Figure 2D**). To monitor simultaneously the late steps of ring contraction and the membrane ingression and fusion, we developed time-lapse experiments of wild-type and *rga7*Δ cells expressing GFP-Psy1 and Rlc1-tdTomato. These experiments revealed that in wild-type cells, plasma membrane ingressed as CAR contracted, and the ring disassembled when membranes fused. In contrast, in *rga7*Δ cells, defects in *rga7*Δ cells CAR integrity during contraction resulted in abnormal membrane ingression that did not always occur straight along the initial division plane as in wild-type cells, but appeared sinuous and wavy. Once CAR contraction finished and membranes fused, the ring split apart and did not disassemble properly, leaving remnants flanking the daughter cell membranes that were not evenly separated by the septum but seemed to get closer to each other at some points (**Figure 2E and 2F**).

Abnormal membrane ingression in *rga7*Δ cells was translated into septum formation defects, as evidenced in the calcofluor-stained cells (**Figure 3A**). Cell wall material deposition on an irregular surface resulted in a nonhomogeneous septum layer across the original division plane (**Figure 3A cell #1 and Movie 1**).

To further analyze how septum completion occurs in *rga7*Δ cells, time-lapse experiments similar to those described above were performed in the presence of sublethal calcofluor concentrations to visualize septum formation and closure without affecting cell viability. In wild-type cells, normal septum closure occurred after ring contraction and, as already mentioned, CAR completely disappeared within 9 min after closure (**Figure 3B**). In 40% of *rga7*Δ cells CAR did not disappear but split apart and septum closure was abnormal and not properly completed. The septum leading edges did not join properly, as they appear at different planes, creating a thicker calcofluor-stained area in the center of the septum (**Figure 3B**). In addition, while in wild-type cells separation already started within 10 min after closure, a high percentage of *rga7*Δ cells showed no indication of cell separation during the same time frame. This defect would explain the high percentage of paired cells observed in *rga7*Δ population, and also the presence of some elongated cells with a single septum, which may have

resumed growth even before separation (**Movie 2**). In summary, delays in ring contraction together with delays in cell separation could be the cause of the high percentage of septated/septating and paired cells (27% and 23% respectively) detected in the absence of Rga7.

Bgs1 and Bgs4 β-glucan synthases are responsible for building the PS and the SS respectively (Cortes et al., 2005; Cortes et al., 2002; Liu et al., 1999). Since *rga7Δ* mutant cells present septum defects we analyzed the localization of these enzymes in cells lacking Rga7. In a wild-type strain, as the septum forms, GFP-Bgs1 is visualized as a membrane ring that moves inwards, following CAR contraction. Accumulation of GFP-Bgs1 at the center of the division site is observed at the end of CAR contraction and, after abscission and membranes separation, GFP-Bgs1 shows homogeneous fluorescence intensity along the daughter membranes (Cortes et al., 2002). In cells lacking Rga7, accumulation of GFP-Bgs1 at the center showed stronger fluorescence intensity and for longer time than in wild-type, as shown by time-lapse experiments (**Figure 3C**). Fluorescence intensity quantification along one of the two membranes that had recently undergone abscission confirmed this observation. (**Figure 3D)**. A similar quantification of GFP-Bgs4 fluorescence did not indicate accumulation of Bgs4 at the center of the daughter membranes (**Figure 3D, lower panels)**. Therefore, the lack of Rga7 caused defects in the membrane localization of Bgs1, the enzyme responsible of the PS glucan synthesis.

Rga7 localization and function depends on its F-BAR domain but not on its GAP catalytic activity

It was recently shown that Rga7 localizes to the growing cell tips and to the cell division site (Arasada and Pollard, 2011). During septation it localizes as a ring to the cell equator and as the CAR constricts, Rga7 is detected as a plaque, like other membrane-associated proteins.

In silico structural analysis of Rga7 showed the presence of a Rho GAP domain at the C-terminus (amino acids 506-695), an F-BAR domain at the N-terminus (amino acids 1-277) and a proline-rich region preceding the GAP domain (amino acids 351-496) (**Figure 4A**). F-BAR domains have been reported to bind membranes and induce membrane curvature and tubulation (Frost et al., 2008).

In order to determine each domain contribution to Rga7 localization and function, we made N-terminus GFP-tagged Rga7 truncations that eliminate: the F-BAR domain, the

proline-rich region or the GAP domain. These Rga7 truncations were expressed in an *rga7*Δ background under the *rga7* native promoter and their localization, expression by western-blotting (**Figure 4B**) and functionality were analyzed. GFP tagging of Rga7 at the N-terminus produces a functional fusion protein (as does the C-terminal GFP tagging) as judged by the wild-type phenotype displayed by cells carrying this fusion protein.

The lack of the F-BAR domain (amino acid residues 1-277) completely abolished Rga7 localization. These results are consistent with a role for the F-BAR domain in the binding of Rga7 to the plasma membrane as described in other proteins (Prouzet-Mauleon et al., 2008). In contrast, deletion of the GAP domain (amino acid residues 506-695) did not cause any effect on the protein localization. Finally, Rga7 lacking the proline-rich region (amino acid residues 351-496) localized to the cell tips and to the cell division site, although the protein fluorescence intensity at those locations was considerably reduced compared to the wild-type protein. Most of the fluorescence was observed in internal structures (**Figure 4C**), suggesting that the proline-rich region might be important for Rga7 transport through the biosynthetic pathway and/or protein stability (as lower protein levels were detected by western blotting).

Since GFP-Rga7ΔF-BAR abolishes Rga7 localization, cells carrying this truncation have similar phenotypes to *rga7*Δ (**Figure 4C**). In contrast, cultures of cells carrying GFP-Rga7ΔGAP showed a reduced percentage of dead cells (3.3±0.47%) and of aberrant septation (3±0.09%) although 9.6± 1.2% of cells still had separation defects. Rga7 GAP domain constitutes more than one fourth of the protein length (189 of 695 amino acids for the whole protein) and its deletion could be causing the separation defects by affecting Rga7 structure or interaction with other cytokinesis proteins. To explore this further, we then constructed an Rga7 GAP-dead point mutant by changing the conserved arginine residue that is essential for the GAP activity to alanine (Zhang et al., 1999) to determine if the GAP activity was necessary for Rga7 role during cytokinesis. R542A mutation eliminated the Rga7 GAP activity as was confirmed by a Rho2-GTP pull-down assay (**Figure S2A**). In addition, GFP fusion to the N-terminus of the Rga7-R542A, showed a GAP-dead mutant protein localization similar to the wild type Rga7. (**Figure 4C).** Finally and importantly, Rga7R542A expressed under the *rga7* promoter in an *rga7*Δ background almost completely abolished the defects observed in

*rga7*Δ cells (**Figure 4D**), supporting the idea that Rga7 roles in cytokinesis are independent of its Rho-GAP activity.

To analyze if the F-BAR domain would be sufficient for Rga7 correct localization and function, we fused the GFP to the 277 N-terminal amino acid residues from Rga7 and checked its localization. This truncated protein was not able to reproduce Rga7 localization (**Figure 4C**). It has been described for other F-BAR-containing proteins that this domain is not sufficient for the protein localization, and requires the C-terminal adjacent region (Takeda et al., 2013). Then, we designed another truncated protein, named Rga7-N-term, which includes the F-BAR domain and the region before the proline-rich domain (amino acids 1-351). This truncated Rga7 version fused to GFP at the N-terminal region, localized to the cell tips and to the cell division site as GFP-Rga7, and almost completely suppressed the *rga7*Δ cytokinesis defects and cell death (**Figure 4B and 4C)**. We hypothesized that maybe the F-BAR domain needs the adjacent amino acids to be able to adopt the correct three-dimensional conformation. Finally, in light of our results, we conclude that Rga7 N-terminal region (amino acids 1-351) including the F-BAR domain is necessary and sufficient for proper Rga7 localization at the cell division site and for its function in the cytokinesis process and cell integrity.

F-BAR domain is necessary for Rga7 localization to the membrane at the cell tips and division site and these domains have been shown to associate with negatively charged lipids such as PI(4,5)P_2 and Phosphatidilserine. Specially, they have been reported to bind to PI(4,5)P_2 enriched at the cell division site (Tsujita et al, 2006; Takeda et al, 2013). We analysed if Rga7 F-BAR domain was responsible for membrane lipid binding and the specificity of this binding by using a protein lipid overlay assay. Purified GST-Rga7 and GST-Rga7ΔF-BAR from fission yeast cells over-expressing these GST-tagged proteins, were used to probe a hydrophobic membrane with different spots of immobilized phospholipids (PIP strips). Full length Rga7 protein strongly bound to PI(4)P and it also bound other monophosphorylated forms of phosphatidylinositols,. In contrast, no lipid binding was observed with the GST-Rga7ΔF-BAR (**Figure 4E**). These results suggest that the F-BAR domain is responsible for membrane binding of Rga7. Recently, PIP4 has been proposed to constitute an essential lipid determinant of plasma membrane identity, independently of its role as a precursor of PI(4,5)P_2 (Hammond et al, Science 2012). It is noteworthy that

S.cerevisiae F-BAR protein Rgd1, also shows strong binding with PI(4)P and this phosphoinositide strongly activates GTP hydrolysis by Rho4, in the presence of Rgd1 (Prouzet-Mauleon et al, 2008).

To see if the role of the F-BAR domain (amino acids 1-277) was simply to localize the N-terminal part of the protein we targeted Rga7 protein lacking the F-BAR domain to the cell division site. We used Pxl1 N-terminal region (1-257 amino acid residues), which localizes to the CAR (Pinar et al., 2008), fused to Rga7 lacking the F-BAR domain (amino acids 277-695). We also fused the Rga7ΔBAR to a GFP tag followed by the nine C-terminal residues that mediate Rho2 targeting to the plasma membrane (amino acids SSTKCCIIS), henceforth called GFP-CAAX. The expression of these GFP-tagged chimeras was analyzed by western blotting and microscopically (**Figures S2B and S2C**). These chimeric proteins localized to the CAR and to the plasma membrane respectively, but none of them was able to suppress the aberrant septation or cell death defects of *rga7*Δ cells (**Figures S2C and S2D).**

Rga7 collaborates with the F-BAR protein Cdc15 in contractile ring stability

Two *S. pombe* proteins containing F-BAR domains, Cdc15 and Imp2, have been implicated in ensuring proper cytokinesis (Arai and Mabuchi, 2002; Balasubramanian et al., 1998; Carnahan and Gould, 2003; Chang et al., 1996; Demeter and Sazer, 1998; Fankhauser et al., 1995). Cdc15 plays an essential role in cytokinesis as it is involved in actomyosin ring assembly and stability during contraction (Wachtler et al., 2006). Imp2, on the other hand, is not essential but contributes to actomyosin ring disassembly (Demeter and Sazer, 1998).

The requirement of the F-BAR domain for Rga7 function during cytokinesis led us to examine whether Rga7 could collaborate with either of the two mentioned F-BAR proteins during this process. We generated the double mutant *rga7*Δ *cdc15-140* and tested its growth at several temperatures. While *cdc15-140* thermosensitive (ts) mutant was able to grow at 32ºC in YES plates, the double mutant *rga7*Δ *cdc15-140* could not grow over 28ºC (**Figure 5A**). In addition, we were not able to obtain *rga7*Δ *imp2*Δ double mutant strain (**Figure 6A**), suggesting that Rga7 collaborates with both F-BAR-containing proteins during cytokinesis.

To further study the *rga7*Δ *cdc15-140* double mutant strain we labelled the cells with Rlc1-tdTomato and Cut11-GFP. *cdc15-140* ts allele led to elongated, multinucleated

cells without a ring and without a division septum when incubated at the restrictive temperature of 36ºC whereas cells looked similar to wild-type at 25ºC. After 3 h of incubation at the semi-permissive temperature of 30ºC, *rga7*Δ *cdc15-140* double mutant cells presented a high percentage of septating cells without CAR (73.6%±3,5) (**Figure 5B and 5C**). In contrast, only the 3.3± 1.1% of *cdc15-140* and none in *rga7*Δ mutant cells showed this defect (**Figure 5B and 5C**). These results suggest that Cdc15 and Rga7 cooperate in the maintenance and stability of the CAR during contraction.

To determine which domains in Rga7 and Cdc15 were responsible for the negative genetic interaction observed in *rga7*Δ *cdc15-140* cells, we first assayed the ability to grow at 28ºC of *rga7*Δ *cdc15-140* double mutants expressing the different *rga7* truncations under the *rga7* native promoter. Cells carrying constructs with the F-BAR domain, *rga7ΔGAP* and *rga7ΔPro*, behaved as *cdc15-140* single mutant. In contrast, cells carrying the rga7*Δ*F-BAR truncation were unable to grow at 28ºC, as the *rga7*Δ *cdc15-140* double mutant. In light of these results, we conclude that the *rga7*Δ *cdc15-140* negative genetic interaction detected is probably due to the loss of the Rga7 F-BAR domain function (**Figure 5D**).

We also checked whether the SH3 domain of Cdc15 was responsible for the negative genetic interaction detected with *rga7Δ*. This domain is involved in recruiting proteins important for the structural integrity of the ring in cooperation with the SH3 domain of Imp2 (Roberts-Galbraith et al., 2009). However, *rga7Δ cdc15Δ*SH3 double mutant cells were able to grow at 28ºC although not as well as *cdc15Δ*SH3 single mutant cells (**Figure S3A**). Therefore, loss of SH3 domain function in *cdc15-140* cells was not responsible for *rga7*Δ *cdc15-140* lethality at 28ºC.

Altogether, these results support the hypothesis that Cdc15 and Rga7 cooperate during fission yeast cytokinesis.

Rga7 and Imp2 collaborate to guarantee proper ring anchoring, integrity, contraction and disassembly

As mentioned before, *rga7Δ imp2Δ* are synthetic lethal and we did not recover any double mutant from a cross between *rga7* and *imp2* deletion strains; Germinating double mutant spores appeared as a single elongated cell with more than one septum. Therefore they likely die due to a defect in cell separation (**Figure 6A**). To study in detail the cytokinesis defects caused by the absence of both proteins we generated a

strain expressing *rga7*$^{+}$ under the control of the thiamine-repressible *P81nmt1* promoter in an *imp2Δ* genetic background which also carried a fluorescently tagged version of Rlc1. After 14 h of growth in thiamine at 25ºC, we could detect phenotypic differences between *imp2Δ*, *P81nmt-rga7*$^{+}$, and *imp2Δ P81nmt-rga7*$^{+}$ double mutant strain, although differences were more dramatic after 20 h in thiamine (**Figure 6B**). Repression of *rga7*$^{+}$ in *imp2Δ* cells led to the appearance of elongated cells with multiple septa, many of which remained uncompleted (63% of septa were uncompleted; n=500 septa). In addition, in many of those uncompleted septa we could not detect the presence of Rlc1-tdTomato rings (39%; n=500 septa), which reminded the phenotype observed in the double *rga7*Δ *cdc15-140* mutant. We also detected the presence of numerous misoriented CARs and septa (16%; n=500 septa) as well as the existence of rings not disassembled (19%) after septation (**Figure 6B**). Time-lapse microscopy observation of these cells showed that some CARs (7%, n=40 CARs) did not contract during the duration of the experiment (120 min.). We also detected Rlc1-tdTomato rings sliding along the cell cortex (3%, n=40 CARs) which suggests that Rga7 and Imp2 act as important anchors of the CAR to the membrane (**Movies 3 and 4**).

To analyze if the presence of multiple and misoriented septa could cause a cut-nuclei phenotype or cell compartments without nucleus, which will cause the cell death, we fixed *imp2Δ P81nmt-rga7*$^{+}$ cells at different times after the addition of thiamine, and stained them with DAPI and calcofluor to visualize the nuclei and cell wall respectively (**Figure S3B**). After 18h of thiamine addition we observed only a small proportion of cut nuclei (3%) a percentage (16%) of cell compartments with 2 or more nuclei and a high frequency of cell compartments without nuclei (62%). These results suggest that cells lacking Imp2 and Rga7 functions, initiate multiple rounds of septation independently of the nuclear division which may cause the cell death when separation occurs.

We also determined which domains in Rga7 and Imp2 were responsible for the synthetic lethality by crossing *imp2*Δ mutant with cells carrying either of the *rga7ΔBAR, rga7ΔGAP,* or *rga7ΔPro* truncations. While *imp2*Δ *rga7ΔGAP* and *imp2*Δ *rga7ΔPro* double mutant cells were viable (**Figure 6C**), we could not obtain *imp2*Δ *rga7ΔBAR* cells (data not shown), which suggests that Rga7 F-BAR and Imp2 functions are redundant in an essential process. In addition, the SH3 domain of Imp2 was not necessary for this process since *rga7*Δ *imp2Δ SH3* strain was viable, although it

presented a reduced growth at high temperatures compared to the single mutants (**Figure S3C**).

Since both Rga7 and Imp2 F-BAR proteins seem to share certain functions during cytokinesis, we checked whether a higher copy number of Rga7 molecules could partially rescue *imp2*Δ growth at restrictive temperature, as cells lacking Imp2 are thermosensitive (Demeter and Sazer, 1998). Transformation of *imp2*Δ cells with the multicopy plasmid pAL-*rga7*$^{+}$ was able to suppress the thermosensitive growth, suggesting that an increased level of Rga7 can substitute for Imp2 (**Figure 6D**). In light of these results we conclude that Rga7 and Imp2 share functions during the cytokinesis process, preventing CAR misorientation and ensuring proper CAR anchoring to the membrane and disassembly.

Rga7 associates with Imp2 and the Imp2 binding partners Fic1 and Pxl1

Cdc15 has been described as one of the earliest proteins to arrive at the ring (Fankhauser et al., 1995; Wu and Pollard, 2005) while Rga7 and Imp2 seem to localize there later (Arasada and Pollard, 2011). In order to compare the timing for appearance of the three F-BAR proteins at the cell division site, we performed time-lapse experiments to monitor Rga7-mCherry and Cdc15-GFP or Imp2-GFP, respectively.

Cdc15 arrived to the cell equator around 12 minutes before Rga7 node-like structures were detectable at this location. Then, Rga7 constituted a proper ring and colocalized with Cdc15. As the CAR contraction occurred, they still colocalized but part of the fluorescent signal corresponding to Rga7-mCherry, extended outside the Cdc15-GFP signal, and the peak of Rga7-mCherry fluorescent signal was behind Cdc15-GFP peak (**Figure 7A**). This is in agreement with the fact that Cdc15-GFP shows a CAR localization and does not form a disk whereas Rga7 forms a disk-like structure as the CAR contracts, like many membrane proteins that localize to the cell equator do. Rga7 seems to arrive to the cell tips and to the cell division site independently of Cdc15 function. However, since lack of Cdc15 function (*cdc15-140* mutant at restrictive temperature) produces unstable CARs, we do not detect Rga7 mature rings in this genetic background but we just can detect Rga7 in "node-like" structures at the cell division site (**Figure S4A and S4B**).

Imp2-GFP and Rga7-mCherry reached the cell equator at the same time and before CAR contraction occurred. When Rga7 node-like structures appeared, a faint Imp2-GFP

ring was detected. Again, during CAR contraction we were able to detect Rga7-mCherry fluorescent signal colocalized with Imp2-GFP at the leading edge of the CAR but behind the GFP signal during contraction (**Figure 7B**).

We also performed co-immunoprecipitation experiments to analyze whether Rga7, Cdc15 and Imp2 could be part of a protein complex. Cells expressing Rga7-3HA and Imp2-GFP revealed an association between these proteins (**Figure 7C)**. However, we could not detect an Rga7-3HA interaction with Cdc15-GFP at endogenous expression levels of the proteins (not shown).

The fact that Rga7 and Imp2 associate and arrive to the cell equator simultaneously, suggests that one could be needed for the other proper localization. However, microscopy observation of either protein (Rga7-GFP and Imp2-GFP) in cells lacking the other (*imp2*Δ and *rga7*Δ) allowed us to discard this possibility (**Figure S4C and S4D**). Imp2, as well as Cdc15, is known to recruit other CAR-associated proteins such as Fic1 and Pxl1 which are important for maintenance of ring integrity (Roberts-Galbraith et al., 2009). Additionally, we identified a synthetic lethal interaction among *rga7*$^{+}$ and *pxl1*$^{+}$ (Supplementary Table 1); therefore, we tested whether Rga7 would also associate with these proteins. Co-immunoprecipitation experiments confirmed Rga7 interaction with Fic1 and Pxl1 (**Figure 7D and 7E**), suggesting that these proteins form part of a complex that tethers the CAR to the membrane and fine-tunes the correct execution of the cytokinesis process.

DISCUSSION

In this study, we have shown how Rga7, an F-BAR and Rho GAP domain-containing protein, plays important roles in fission yeast cytokinesis, ensuring actomyosin ring stability during contraction, proper ring disassembly, correct septation, and cell separation. In addition, we demonstrated that Rga7 localization and its function in cytokinesis are not dependent on its GAP activity but depends on the F-BAR domain and the contiguous region of the protein. Some F-BAR domains have been involved in linking the plasma membrane to the cytoskeleton (Aspenstrom, 2009; Itoh et al., 2005; Tsujita et al., 2006). Rga7 localization and the presence of an F-BAR domain at its N-terminus suggest that this membrane-associated protein could be part of an anchor for the CAR to the plasma membrane during contraction. Defective CAR anchoring to the membrane could cause the observed CARs with irregular morphology in *rga7*Δ cells. These CARs would guide the irregular membrane ingression and consequently the

irregular primary septum synthesis. In many cases, as judged by the calcofluor staining, the septum is not synthesized homogeneously and in a straight division plane as in wild-type cells. This irregular septum is likely the cause of the cell separation defects observed in cells lacking Rga7 since it may obstruct the advance or action of the septum-degrading enzymes, such as Eng1 or Agn1 (Garcia et al., 2005; Hochstenbach et al., 1998; Martin-Cuadrado et al., 2003). Cell death observed in *rga7*Δ could also be caused by these septa and membrane defects during separation, since most of the dead cells observed are paired cells.

Several membrane-associated proteins have been shown to ensure CAR integrity, including the F-BAR-containing proteins Cdc15 and Imp2 that bind to the CAR or the equatorial membrane (Celton-Morizur et al., 2004; Martin-Garcia and Valdivieso, 2006; Roberts-Galbraith et al., 2009). We have found that Rga7 cooperates with Cdc15 and Imp2 in maintaining CAR stability, especially during contraction, as judged by the presence of uncompleted septa without CAR, when the function of Rga7 and Cdc15 or Imp2 is simultaneously affected. Indeed, we detected co-immunoprecipitation of Rga7 with Imp2 and with Pxl1 and Fic1, two CAR components that bind to Cdc15 and Imp2 through the SH3 domain. Thus, as F-BAR domain-containing proteins, Rga7, Cdc15 and Imp2 could collaborate in safeguarding the linkage of the plasma membrane to the CAR. High redundancy of proteins mediating CAR tethering to the membrane may be necessary especially during contraction, when forces pulling and pushing the plasma membrane are generated from the CAR and the septum respectively.

Simultaneous localization of Rga7 and Cdc15 or Imp2 during ring contraction revealed that Rga7 remains along the equatorial membrane while Cdc15 and Imp2 localization is more characteristic of CAR proteins, suggesting that they are restricted to the membrane leading edge. This localization could reflect a different function of these proteins as occurs with the F-BAR proteins srGAP1, srGAP2 and srGAP, which show differential localization within cortical neurons filopodial protrusions and so, differentially regulate membrane deformation in these neurons (Coutinho-Budd et al., 2012). Generation of distinct curvatures would be in agreement with a role for Cdc15, Imp2 and Rga7 at diverse stages of cytokinesis, and with a differential localization at the invaginated plasma membrane. Cells lacking Rga7 show defects mainly during the final steps of cytokinesis, when membrane fusion and abscission take place. Membrane curvature has long been believed an important modulator of the membrane fusion process (Kasson and Pande, 2007). It is tempting to think that the Rga7 F-BAR domain ensures the

proper membrane curvature important for the last steps of cytokinesis. Fluorescence and electron microscopy analysis revealed defects at the center of the primary septum in *rga7*Δ cells. The time-lapse experiments performed suggest that the observed defects are due to problems in membrane fusion and septum closure. Concomitantly, the CAR does not disassemble properly and this could be the cause of the septum closure defects. A similar defect in final stages of septum formation has been described in Anaphase Promoting Complex (APC) mutants in budding yeast, which also show defects in CAR disassembly (Tully et al., 2009). However, other mutant strains affected in ring disassembly, such as *myp2Δ, fic1Δ or imp2Δ* (Bohnert and Gould, 2012; Demeter and Sazer, 1998), do not show these septum completion defects. Therefore Rga7 might have a role in ring disassembly at the correct time of cytokinesis different from that of the proteins mentioned above. Alternatively, the failure to disassemble the ring components may be a consequence, rather than a cause, of a defect in membrane or septum closure.

In summary, Rga7 seems to be part of a protein complex which ensures contractile ring integrity and anchorage to the membrane. Such proteins could provide some functional redundancy to the molecular mechanism underlying this important process. It is likely that other proteins form part of this complex and their identification and the determination of their contribution to this process remain as an important challenge. An exciting possibility is that other F-BAR domain-containing proteins, such as Rga8, which also localizes to the cell division site (Arasada and Pollard, 2011), have a cooperative role with proteins in this complex to fine-tune cytokinesis.

MATERIALS AND METHODS

Strains, growth conditions and genetic methods

Standard *S. pombe* media and genetic manipulations were performed as described (Moreno et al., 1991). All the strains used were isogenic to wild-type strains 972 h^- and 975 h^+, and they are described in Supplemental Table 2. The strains were constructed by either tetrad dissection or random spore germination method. Cells were grown in rich medium (YES) or minimal medium (EMM) supplemented with the necessary requirements. *Escherichia coli* DH5α was used as host for propagation of plasmids. Cells were grown in LB medium supplemented with 50 μg ml^{-1} ampicillin when appropriate. Solid media contained 2% agar.

Recombinant DNA methods

All general techniques have been described previously (Sambrook, 2001). Enzymes were used according to the recommendations of the suppliers. *S. pombe* was transformed by the lithium acetate method (Ito et al., 1983).

Genomic versions of *rga7*$^+$ tagged with the Green Fluorescent Protein (GFP) fused either at the 5′end or the 3′end of the open reading frame (ORF) were generated by cloning the *rga7*$^+$ ORF and the GFP sequence, plus 500 base pairs of the 5′and 3′*rga7*$^+$ flanking sequences into a KS BlueScript. The 5′and 3′ *rga7*+ flanking sequences as well as the *rga7*$^+$ ORF were amplified from the fission yeast genomic DNA using the appropriate primers. Truncated *rga7*ΔF-BAR, *rga7*ΔGAP, *rga7*ΔPro, *rga7*-F-BAR, *rga7* N-terminal were generated by amplifying the corresponding ORF fragments using the appropriate primers and cloning these fragments into a KS Blue Script plasmid carrying the 5′and 3′flanking *rga7*$^+$ sequences. The fidelity of *rga7*$^+$ sequences was confirmed by DNA sequencing. For GFP-tagged versions of *rga7* truncations GFP was ligated at the 5′ of these fragments. All the previous resulting constructs were cloned into the integrative vector pJK148 which was then cut with *Tth11I* and integrated at the *leu1*$^+$ locus of the *leu1-32 ura4-D18 rga7Δ* strain. Transformant clones were selected in EMM without leucine and screened by PCR for the appropriate gene integration.

The *rga7* GAP-dead mutant was generated by PCR site-directed mutagenesis using the Pfu Ultra High Fidelity Polymerase (*Agilent Technologies*), the appropriate primers and a KS Bluescript containing the *rga7*$^+$ ORF as template. Substitution of the arginine residue 542 for alanine was confirmed by DNA sequencing. The mutated *rga7* ORF was then cloned into pJK148 and integrated into the *leu1*$^+$ locus of the *leu1-32 ura4-D18 rga7Δ* strain as described before.

Generation of pxl1N-term-rga7ΔF-BAR chimera was performed amplifying the *rga7ΔF-BAR* fragment using appropriate primers, which was then ligated to the *NdeI-NheI* fragment containing the *pxl1*$^+$ N-terminal region (obtained from a lab stock plasmid) between the 5′and 3′ *rga7*$^+$ non-coding flanking regions in KS Bluescript vector (digested with *NdeI-BamHI)*. The resulting construct was then cloned into pJK148 for chromosome integration as previously described.

Tagging of Rga7 at its C-terminus with GFP-CAAX was performed by PCR amplification of the coding sequence for the GFP followed by the nine terminal aa′ of fission yeast Rho2 and a STOP codon, using the appropriate primers and the genomic DNA from a Rho2-GFP strain which carries the GFP just before these nine terminal aa′.

The *BamHI-BamHI* amplified fragment was cloned at the 3´end of the *rga7*ΔBAR ORF in a pJK148 vector which was then integrated in the *leu1-32 ura4-D18 rga7*Δ strain following the strategy previously mentioned.

rga7 and *rga7ΔF-BAR* were cloned into the pDS472a vector as a *PstI-NotI* fragment for over expression and purification of these GST tagged proteins from fission yeast.

P81nmt-3HA-*rga7*$^{+}$ and Rga7-mCherry:*natMX6* strains were created using appropriate templates and primers as described (Bahler et al., 1998).

Purification of fission yeast GST fusion protein and Protein Lipid Overlay Assay

The *rga7*Δ strains expressing the plasmid pDS472a rga7-GST or the pDS472a-rga7ΔF-BAR-GST were cultured in the absence of thiamine to induce the expression of these proteins. Cells were disrupted with glass beads in lysis buffer (50 mM Tris-HCl pH 8, 100 mM NaCl, 0.1% Triton, protease inhibitor cocktail and PMSF). Protein extracts incubated for 2h at 4ºC with Glutathione-Sepharose beads (*GE Healthcare*) were washed with lysis buffer and GST fusion proteins were eluted with elution buffer (lysis buffer containing 20mM reduced glutathione). Immobilized phospholipids membranes (PIP strips from *Echelon Biosciences*) were blocked with 1% nonfat milk in TBST for 1h. Then, 500 µg of Rga7 or Rga7ΔF-BAR were added to blocking solution and incubated with the PIP strips for 1h. After washing with TBST, the PIP strips were incubated with 1:10000 dilution anti-GST antibody HRP conjugated (*GE Healthcare*). The membrane was washed and bound antibodies were detected by chemiluminiscence.

Microscopy

Fluorescence images were captured on an inverted microscope (model IX71; Olympus) equipped with a PlanApo 100x/1.40 IX70 objective and a Personal DeltaVision system (Applied Precision). Images were captured using a CoolSnap HQ2 monochrome camera (Photometrics) and softWoRx 5.5.0 imaging software (Applied Precision). For 3-dimensional reconstructions of the ring and septum, 22-24 z-planes, 0.2 µm apart, were taken along the cell width. All fluorescent images were then corrected by 3-D deconvolution (conservative ratio, 10 iterations and medium noise filtering) using the softWoRx imaging software. Next, images were processed with ImageJ (National Institutes of Health, Bethesda, MD).

For time-lapse imaging, 0.3 ml of log-phase cell cultures were placed in a well from a µ-Slide 8 well (*Ibidi*) previously coated with 10 µl of 2 mg/ml soybean lectin (*Sigma-Aldrich*) as described (Cortes et al., 2012).

Time-lapse experiments were made at 32°C and single middle planes were taken every 3 minutes using a thermostatic chamber coupled to the microscope.

DAPI staining was performed on cells fixed with 70% ethanol as described (Moreno et al., 1991).

Electron microscopy was performed on permanganate-stained cells as described (Konomi et al., 2003). Ultrathin sections were cut on a Jung Reichert microtome (*Leica Mikroskopie and System GmbH*) and examined using a JEM1010 transmission electron microscope (Jeol) at 100 kV.

Other methods

For plate growth test, early log-phase cells growing at 25°C were adjusted at OD_{600}=1 or OD_{600}=4 and serially diluted 1:4. Then cells were spotted onto YES or EMM-leu, and incubated for 2–3 days at the indicated temperatures.

AKNOWLEDGEMENTS

We thank J.C. Cortés, J. Encinar, and S. Rincón for thoughtful comments and D. Posner for language revision. We thank K. Gould, I. Mabuchi, J. Moseley, J.C. Ribas, and H. Valdivieso for strains. R. Martín-García was funded by a contract JAEDOC023 from CSIC. This work was supported by Grant BFU2010-15641 from Ministerio de Economía y Competitividad, Spain.

REFERENCES

Arai, R. and Mabuchi, I. (2002). F-actin ring formation and the role of F-actin cables in the fission yeast Schizosaccharomyces pombe. *J Cell Sci* **115**, 887-98.

Arasada, R. and Pollard, T. D. (2011). Distinct roles for F-BAR proteins Cdc15p and Bzz1p in actin polymerization at sites of endocytosis in fission yeast. *Curr Biol* **21**, 1450-9.

Aspenstrom, P. (2009). Roles of F-BAR/PCH proteins in the regulation of membrane dynamics and actin reorganization. *Int Rev Cell Mol Biol* **272**, 1-31.

Bahler, J., Wu, J. Q., Longtine, M. S., Shah, N. G., McKenzie, A., 3rd, Steever, A. B., Wach, A., Philippsen, P. and Pringle, J. R. (1998). Heterologous modules for efficient and versatile PCR-based gene targeting in Schizosaccharomyces pombe. *Yeast* **14**, 943-51.

Balasubramanian, M. K., Bi, E. and Glotzer, M. (2004). Comparative analysis of cytokinesis in budding yeast, fission yeast and animal cells. *Curr Biol* **14**, R806-18.

Balasubramanian, M. K., McCollum, D., Chang, L., Wong, K. C., Naqvi, N. I., He, X., Sazer, S. and Gould, K. L. (1998). Isolation and characterization of new fission yeast cytokinesis mutants. *Genetics* **149**, 1265-75.

Barr, F. A. and Gruneberg, U. (2007). Cytokinesis: placing and making the final cut. *Cell* **131**, 847-60.

Bi, E. (2001). Cytokinesis in budding yeast: the relationship between actomyosin ring function and septum formation. *Cell Struct Funct* **26**, 529-37.

Bohnert, K. A. and Gould, K. L. (2012). Cytokinesis-based constraints on polarized cell growth in fission yeast. *PLoS Genet* **8**, e1003004.

Carnahan, R. H. and Gould, K. L. (2003). The PCH family protein, Cdc15p, recruits two F-actin nucleation pathways to coordinate cytokinetic actin ring formation in Schizosaccharomyces pombe. *J Cell Biol* **162**, 851-62.

Celton-Morizur, S., Bordes, N., Fraisier, V., Tran, P. T. and Paoletti, A. (2004). C-terminal anchoring of mid1p to membranes stabilizes cytokinetic ring position in early mitosis in fission yeast. *Mol Cell Biol* **24**, 10621-35.

Cortes, J. C., Carnero, E., Ishiguro, J., Sanchez, A., Duran, A. and Ribas, J. C. (2005). The novel fission yeast (1,3)beta-D-glucan synthase catalytic subunit Bgs4p is essential during both cytokinesis and polarized growth. *J Cell Sci* **118**, 157-74.

Cortes, J. C., Ishiguro, J., Duran, A. and Ribas, J. C. (2002). Localization of the (1,3)beta-D-glucan synthase catalytic subunit homologue Bgs1p/Cps1p from fission yeast suggests that it is involved in septation, polarized growth, mating, spore wall formation and spore germination. *J Cell Sci* **115**, 4081-96.

Cortes, J. C., Konomi, M., Martins, I. M., Munoz, J., Moreno, M. B., Osumi, M., Duran, A. and Ribas, J. C. (2007). The (1,3)beta-D-glucan synthase subunit Bgs1p is responsible for the fission yeast primary septum formation. *Mol Microbiol* **65**, 201-17.

Cortes, J. C., Sato, M., Munoz, J., Moreno, M. B., Clemente-Ramos, J. A., Ramos, M., Okada, H., Osumi, M., Duran, A. and Ribas, J. C. (2012). Fission yeast Ags1 confers the essential septum strength needed for safe gradual cell abscission. *J Cell Biol* **198**, 637-56.

Coutinho-Budd, J., Ghukasyan, V., Zylka, M. J. and Polleux, F. (2012). The F-BAR domains from srGAP1, srGAP2 and srGAP3 regulate membrane deformation differently. *J Cell Sci* **125**, 3390-401.

Chang, F., Woollard, A. and Nurse, P. (1996). Isolation and characterization of fission yeast mutants defective in the assembly and placement of the contractile actin ring. *J Cell Sci* **109 (Pt 1)**, 131-42.

Chitu, V. and Stanley, E. R. (2007). Pombe Cdc15 homology (PCH) proteins: coordinators of membrane-cytoskeletal interactions. *Trends Cell Biol* **17**, 145-56.

Demeter, J. and Sazer, S. (1998). imp2, a new component of the actin ring in the fission yeast Schizosaccharomyces pombe. *J Cell Biol* **143**, 415-27.

Fankhauser, C., Reymond, A., Cerutti, L., Utzig, S., Hofmann, K. and Simanis, V. (1995). The S. pombe cdc15 gene is a key element in the reorganization of F-actin at mitosis. *Cell* **82**, 435-44.

Frost, A., Perera, R., Roux, A., Spasov, K., Destaing, O., Egelman, E. H., De Camilli, P. and Unger, V. M. (2008). Structural basis of membrane invagination by F-BAR domains. *Cell* **132**, 807-17.

Frost, A., Unger, V. M. and De Camilli, P. (2009). The BAR domain superfamily: membrane-molding macromolecules. *Cell* **137**, 191-6.

Garcia, I., Jimenez, D., Martin, V., Duran, A. and Sanchez, A. (2005). The alpha-glucanase Agn1p is required for cell separation in Schizosaccharomyces pombe. *Biol Cell* **97**, 569-76.

Guertin, D. A., Trautmann, S. and McCollum, D. (2002). Cytokinesis in eukaryotes. *Microbiol Mol Biol Rev* **66**, 155-78.

Hammond, G. R., Fischer, M. J., Anderson, K. E., Holdich, J., Koteci, A., Balla, T. and Irvine, R. F. (2012) PI4P and PI(4,5)P2 are essential but independent lipid determinants of membrane identity. *Science* **337**, 727-30.

Hochstenbach, F., Klis, F. M., van den Ende, H., van Donselaar, E., Peters, P. J. and Klausner, R. D. (1998). Identification of a putative alpha-glucan synthase essential for cell wall construction and morphogenesis in fission yeast. *Proc Natl Acad Sci U S A* **95**, 9161-6.

Ito, H., Fukuda, Y., Murata, K. and Kimura, A. (1983). Transformation of intact yeast cells treated with alkali cations. *J Bacteriol* **153**, 163-8.

Itoh, T., Erdmann, K. S., Roux, A., Habermann, B., Werner, H. and De Camilli, P. (2005). Dynamin and the actin cytoskeleton cooperatively regulate plasma membrane invagination by BAR and F-BAR proteins. *Dev Cell* **9**, 791-804.

Kasson, P. M. and Pande, V. S. (2007). Control of membrane fusion mechanism by lipid composition: predictions from ensemble molecular dynamics. *PLoS Comput Biol* **3**, e220.

Konomi, M., Fujimoto, K., Toda, T. and Osumi, M. (2003). Characterization and behaviour of alpha-glucan synthase in Schizosaccharomyces pombe as revealed by electron microscopy. *Yeast* **20**, 427-38.

Lippincott, J. and Li, R. (2000). Involvement of PCH family proteins in cytokinesis and actin distribution. *Microsc Res Tech* **49**, 168-72.

Liu, J., Wang, H., McCollum, D. and Balasubramanian, M. K. (1999). Drc1p/Cps1p, a 1,3-beta-glucan synthase subunit, is essential for division septum assembly in Schizosaccharomyces pombe. *Genetics* **153**, 1193-203.

Martin-Cuadrado, A. B., Duenas, E., Sipiczki, M., Vazquez de Aldana, C. R. and del Rey, F. (2003). The endo-beta-1,3-glucanase eng1p is required for dissolution of the primary septum during cell separation in Schizosaccharomyces pombe. *J Cell Sci* **116**, 1689-98.

Martin-Garcia, R. and Valdivieso, M. H. (2006). The fission yeast Chs2 protein interacts with the type-II myosin Myo3p and is required for the integrity of the actomyosin ring. *J Cell Sci* **119**, 2768-79.

Moreno, S., Klar, A. and Nurse, P. (1991). Molecular genetic analysis of fission yeast *Schizosaccharomyces pombe*. *Methods Enzymol* **194**, 795-823.

Munoz, J., Cortes, J. C., Sipiczki, M., Ramos, M., Clemente-Ramos, J. A., Moreno, M. B., Martins, I. M., Perez, P. and Ribas, J. C. (2013). Extracellular cell wall beta(1,3)glucan is required to couple septation to actomyosin ring contraction. *J Cell Biol* **203**, 265-82.

Pinar, M., Coll, P. M., Rincon, S. A. and Perez, P. (2008). Schizosaccharomyces pombe Pxl1 is a paxillin homologue that modulates Rho1 activity and participates in cytokinesis. *Mol Biol Cell* **19**, 1727-38.

Pollard, T. D. and Wu, J. Q. (2010). Understanding cytokinesis: lessons from fission yeast. *Nat Rev Mol Cell Biol* **11**, 149-55.

Proctor, S. A., Minc, N., Boudaoud, A. and Chang, F. (2012). Contributions of turgor pressure, the contractile ring, and septum assembly to forces in cytokinesis in fission yeast. *Curr Biol* **22**, 1601-8.

Prouzet-Mauleon, V., Lefebvre, F., Thoraval, D., Crouzet, M. and Doignon, F. (2008). Phosphoinositides affect both the cellular distribution and activity of the F-BAR-containing RhoGAP Rgd1p in yeast. *J Biol Chem* **283**, 33249-57.

Roberts-Galbraith, R. H., Chen, J. S., Wang, J. and Gould, K. L. (2009). The SH3 domains of two PCH family members cooperate in assembly of the Schizosaccharomyces pombe contractile ring. *J Cell Biol* **184**, 113-27.

Roberts-Galbraith, R. H. and Gould, K. L. (2010). Setting the F-BAR: functions and regulation of the F-BAR protein family. *Cell Cycle* **9**, 4091-7.

Sambrook, J. a. R., D.W. (2001). Molecular cloning: A laboratory Manual. Cold Spring Harbor, New York: Cold Spring Harbor Laboratory Press.

Soto, T., Villar-Tajadura, M. A., Madrid, M., Vicente, J., Gacto, M., Perez, P. and Cansado, J. (2010). Rga4 modulates the activity of the fission yeast cell integrity MAPK pathway by acting as a Rho2 GTPase-activating protein. *J Biol Chem* **285**, 11516-25.

Takeda, T., Robinson, I. M., Savoian, M. M., Griffiths, J. R., Whetton, A. D., McMahon, H. T. and Glover, D. M. (2013). Drosophila F-BAR protein Syndapin contributes to coupling the plasma membrane and contractile ring in cytokinesis. *Open Biol* **3**, 130081.

Tsujita, K., Suetsugu, S., Sasaki, N., Furutani, M., Oikawa, T. and Takenawa, T. (2006). Coordination between the actin cytoskeleton and membrane deformation by a novel membrane tubulation domain of PCH proteins is involved in endocytosis. *J Cell Biol* **172**, 269-79.

Tully, G. H., Nishihama, R., Pringle, J. R. and Morgan, D. O. (2009). The anaphase-promoting complex promotes actomyosin-ring disassembly during cytokinesis in yeast. *Mol Biol Cell* **20**, 1201-12.

Wachtler, V., Huang, Y., Karagiannis, J. and Balasubramanian, M. K. (2006). Cell cycle-dependent roles for the FCH-domain protein Cdc15p in formation of the actomyosin ring in Schizosaccharomyces pombe. *Mol Biol Cell* **17**, 3254-66.

Wu, J. Q., Kuhn, J. R., Kovar, D. R. and Pollard, T. D. (2003). Spatial and temporal pathway for assembly and constriction of the contractile ring in fission yeast cytokinesis. *Dev Cell* **5**, 723-34.

Wu, J. Q. and Pollard, T. D. (2005). Counting cytokinesis proteins globally and locally in fission yeast. *Science* **310**, 310-4.

Yu, H. and Schulten, K. (2013). Membrane sculpting by F-BAR domains studied by molecular dynamics simulations. *PLoS Comput Biol* **9**, e1002892.

Zhang, B., Zhang, Y., Collins, C. C., Johnson, D. I. and Zheng, Y. (1999). A built-in arginine finger triggers the self-stimulatory GTPase-activating activity of rho family GTPases. *J Biol Chem* **274**, 2609-12.

FIGURE LEGENDS

Figure 1. Rga7 functions in morphogenesis, cytokinesis and cell integrity.
(A) Representative images from wild-type (wt) and *rga7*Δ cells grown in YES at 32ºC (left and middle panel) or 36ºC (right panel) and stained with calcofluor. Arrowheads mark aberrant septa with a thick region, asterisks indicate cells exhibiting cell separation defects (paired cells), and the arrow points to an abnormally elongated and septated cell. Cells in the inset (middle panel, upper-left side) correspond to another image from the same strain which has been included to visualize nonhomogeneous calcofluor staining of the septa. (B) Quantification of the phenotypes observed in (A). Wild-type cells grown at 36ºC are not shown to simplify the figure since they were similar to those grown at 32ºC. Horizontal lines represent normal septating/septated cells; cells with septation defects have been divided into two types: multiseptated or cells with aberrant morphology septum. Quantifications were taken from three independent experiments (n=250 for each strain and experiment). Mean percentages are represented; Standard deviations for these values are not represented here for simplicity but they are stated in the text. (C) calcofluor stained and electron micrographs from septum region of wild-type (i and ii) and *rga7Δ* (iii to viii) cells grown in YES at 32ºC. Scale Bars: 5 μm (A) or 0.5 μm (C).

Figure 2. Rga7 ensures actomyosin ring integrity and proper ring disassembly.
(A) Live cell images from wild-type (wt) and *rga7Δ* cells expressing GFP-Psy1 and Rlc1-tdTomato (single focal planes). The inset shows the magnified region inside the white box. (B) Frontal (upper and middle panels) and lateral views (bottom) of three-dimensional maximum projection reconstructions from wt and *rga7Δ* contractile rings at the indicated temperatures. (C) Time-lapse images of wild-type (wt) and *rga7Δ* cells grown and imaged at 32ºC. Rlc1-tdTomato serves as a ring marker. Images were acquired at 3-min intervals at the medial focal plane. (D) Quantification of timing for ring contraction (graph on the left) as the time from start of contraction to ring closure in wild-type and *rga7Δ* cells expressing Rlc1-tdTomato and Cut11-GFP. n=20 for each strain. Data are presented in box and whisker plots showing the mean (black dot in the box), the median (line in the box), 25^{th}–75^{th} percentiles (box) and 5^{th}–95^{th} percentiles (whiskers) for each strain. Timing for ring contraction in mutant cells is significantly different from wild type cells by Student´s t-test with $p<0.05$ (*). Quantification of

timing for ring disassembly (graph on the right) as the interval from ring closure to ring signal disappearance in the same cells as described above. n=20 for each genotype. Data are also presented in box and whisker plots. Cells taking longer than 60 min to disassemble the ring were not considered. Timing for ring disassembly in mutant cells is significantly different from wild type cells by Student´s t-test with $p<0.01$ (**). (E) Time-lapse images showing final steps of ring contraction in wt and *rga7Δ* cells expressing Rlc1-tdTomato and GFP-Psy1. Images were taken at 3-min intervals. Right panels show magnified images from *rga7*Δ cell equator with ring remnants flanking the membranes. (F) Fluorescence images (single focal plane) of GFP-Psy1 from wt (upper panel) and *rga7*Δ (bottom panel). Arrows point to the abnormal membranes in *rga7Δ* daughter cells after division. Scale Bars: 5 µm.

Figure 3. Rga7 is necessary for the correct primary septum formation

(A) Fluorescent images from three cells lacking *rga7*$^{+}$ expressing GFP-Psy1, Rlc1-tdTomato and stained with calcofluor. Whole cell images are single z-planes (cell 1, 2 and 3), while magnified images from the equatorial cell region correspond to lateral (top) or frontal (bottom) views of the 3-D maximum projection reconstruction of the cell from multiple z-planes (cell 1). (B) Time-lapse images of wt and *rga7*Δ cells expressing Rlc1-tdTomato stained with calcofluor to monitor ring contraction and septum formation. Images were taken at 5-min intervals. The asterisk indicates two daughter cells that have started separation. (C) Live cell images from wt and *rga7*Δ strains expressing GFP-Bgs1. Cytokinesis late points from time-lapse experiments are shown, with 5-min delay between frames. (D) Scan of the fluorescence intensity along the line drawn across one of the daughter cells membrane in wt and *rga7Δ* expressing GFP-Bgs1 or GFP-Bgs4. Scale Bars: 5 µm.

Figure 4. Rga7 F-BAR domain is necessary for the correct protein localization and function in cytokinesis

(A) Schematic domain representation of Rga7 and different protein truncations generated. (B) Expression levels of GFP-Rga7 and the different GFP-tagged Rga7 versions shown in A determined by Western-Blot. Actin levels were used as loading control. (C) Localization of GFP-tagged Rga7 and the protein truncations generated; asterisks in the third panel indicate GFP-Rga7ΔPro localization to the cell equator and arrowheads mark this protein's faint localization to the cell tips. Scale bar: 5 µm. (D)

Quantification of phenotypes from cells expressing these truncations. Percentage values represent the mean for three independent experiments (n=250 cells per genotype and experiment). (E) Interaction of Rga7 and Rga7ΔF-BAR with phospholipids as revealed by protein-lipid overlay assay.

Figure 5. Rga7 genetically interacts with the F-BAR protein Cdc15

(A) Plate growth assay of *rga7Δ cdc15-140* double mutant strain and the control strains: wild-type (wt), *rga7Δ,* and *cdc15-140*. Cells were grown to mid-log phase in YES at 25ºC and spotted on plates at OD_{600} 1 and serial 1:4 dilutions. Plates were incubated for 2-3 days at the indicated temperatures. (B) Fluorescence images from calcofluor stained *rga7Δ, cdc15-140* and *rga7Δ cdc15-140* double mutant strain expressing Rlc1-tdTomato and Cut11-GFP to visualize the ring and the nuclear membrane respectively. Cells were grown at 25ºC and then shifted to 30ºC for 3 h before imaging. Binucleated cells with no complete septum and without a contractile actomyosin ring are indicated (arrows). Binucleated cells with no septum and without a CAR are also indicated (arrowheads). Scale Bar: 5 μm. (C) Quantification of binucleated cells without a complete septum and no actomyosin ring. Percentage values represent the mean for three independent experiments (n=200 cells per genotype and experiment). Bars corresponding to the Standard Deviation are also shown. (D). Plate growth assay of *cdc15-140* control cells and *rga7Δ cdc15-140* mutant expressing different Rga7 truncations described in Figure 4A.

Figure 6. Rga7 genetically interacts with the F-BAR protein Imp2

(A) *imp2::ura4* and *rga7::kanMX6* strains were crossed and tetrads pulled and germinated at 25ºC in YES. Circles indicate double mutants not able to grow (right panel). TT: Tetratype; NP: Non-parental ditype; PD: Parental ditype. Images from colonies corresponding to each genotype of a tetratype tetrad are shown (left panel). (B) Fluorescence images of calcofluor (CF)-stained *imp2*Δ *P81nmt-3HA-rga7*$^{+}$ cells expressing Rlc1-tdTomato grown at 25ºC in EMM plus thiamine for 20h (top panels). Arrows indicate the miss-oriented rings and/or septa. Asterisks mark those incomplete septa without the presence of a contractile actomyosin ring. The bottom panels represent fluorescence images of the control cells: *imp2*Δ grown in EMM at 25ºC; *imp2*Δ *P81nmt-3HA-rga7*$^{+}$ cells grown in the absence of thiamine at 25ºC; and *P81nmt-3HA-rga7*$^{+}$ cells grown at 25ºC in EMM plus thiamine for 20 h. (C) Plate growth assay of

*imp2*Δ, *imp2*Δ *rga7ΔGAP, and imp2*Δ *rga7ΔPro* mutant strains and the corresponding control strains. (D) Expression of *rga7*$^{+}$ in a multicopy plasmid partially suppresses the *imp2*Δ thermosensitivity. Wild-type and *imp2*Δ strains transformed with pAL or pAL-*rga7* were grown in EMM-leu medium at 25ºC and spotted on the same medium plates at OD_{600} 4 and 1:4 serial dilutions. Plates were incubated for 2−3 days at 25ºC and 36ºC.

Figure 7. Rga7 associates with Imp2 and the Imp2 binding parterns, Fic1 and Pxl1
Time-lapse (6-min interval images) from cells expressing Rga7-mCherry and either Cdc15-GFP (A), or Imp2-GFP (B). On the right, a magnification image of the cell equator region is shown and the graph below represents the fluorescence scan in both channels along a line drawn at this region. (C) Interaction of Rga7 with Imp2. Extracts from cells carrying Rga7-3HA and Imp2-GFP, expressed at endogenous levels were immunoprecipitated with anti-GFP antibody and probed with anti-HA antibody. Extracts were assayed for total levels of Rga7-3HA and Imp2-GFP. (D) Extracts from cells carrying Rga7-3HA and Fic1-GFP, expressed at endogenous levels were immunoprecipitated with anti-HA antibody and probed with anti-GFP antibody. Extracts were assayed for total levels of Rga7-3HA and Fic1-GFP. (E) Interaction of Rga7 and Pxl1. Extracts from cells expressing Rga7-GFP and HA-Pxl1 at endogenous levels were immunoprecipitated with anti-HA antibody and probed with anti-GFP antibody. Extracts were assayed for levels of Rga7-GFP and HA-Pxl1 by Western blot.

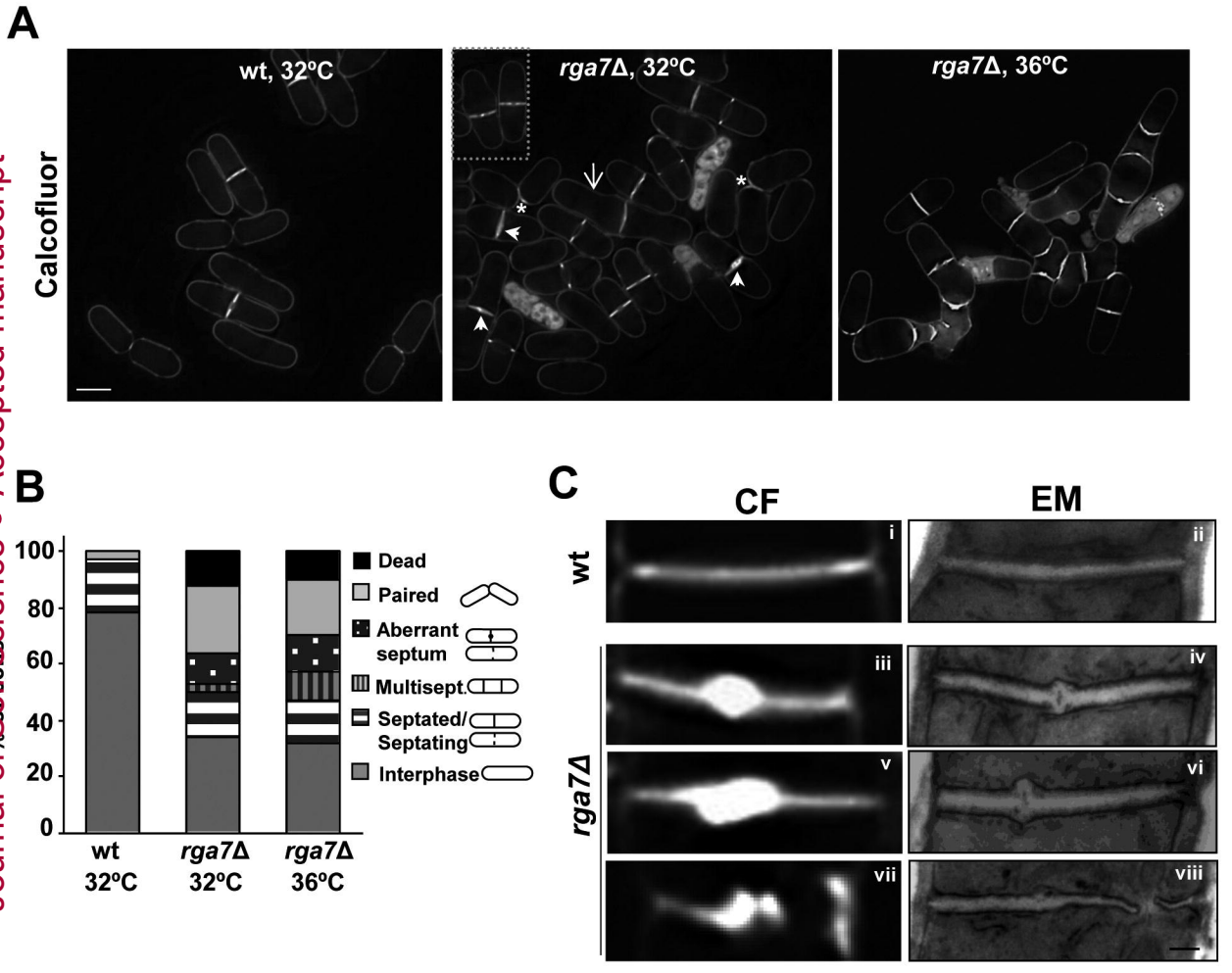

Martín-García et al., Figure 1

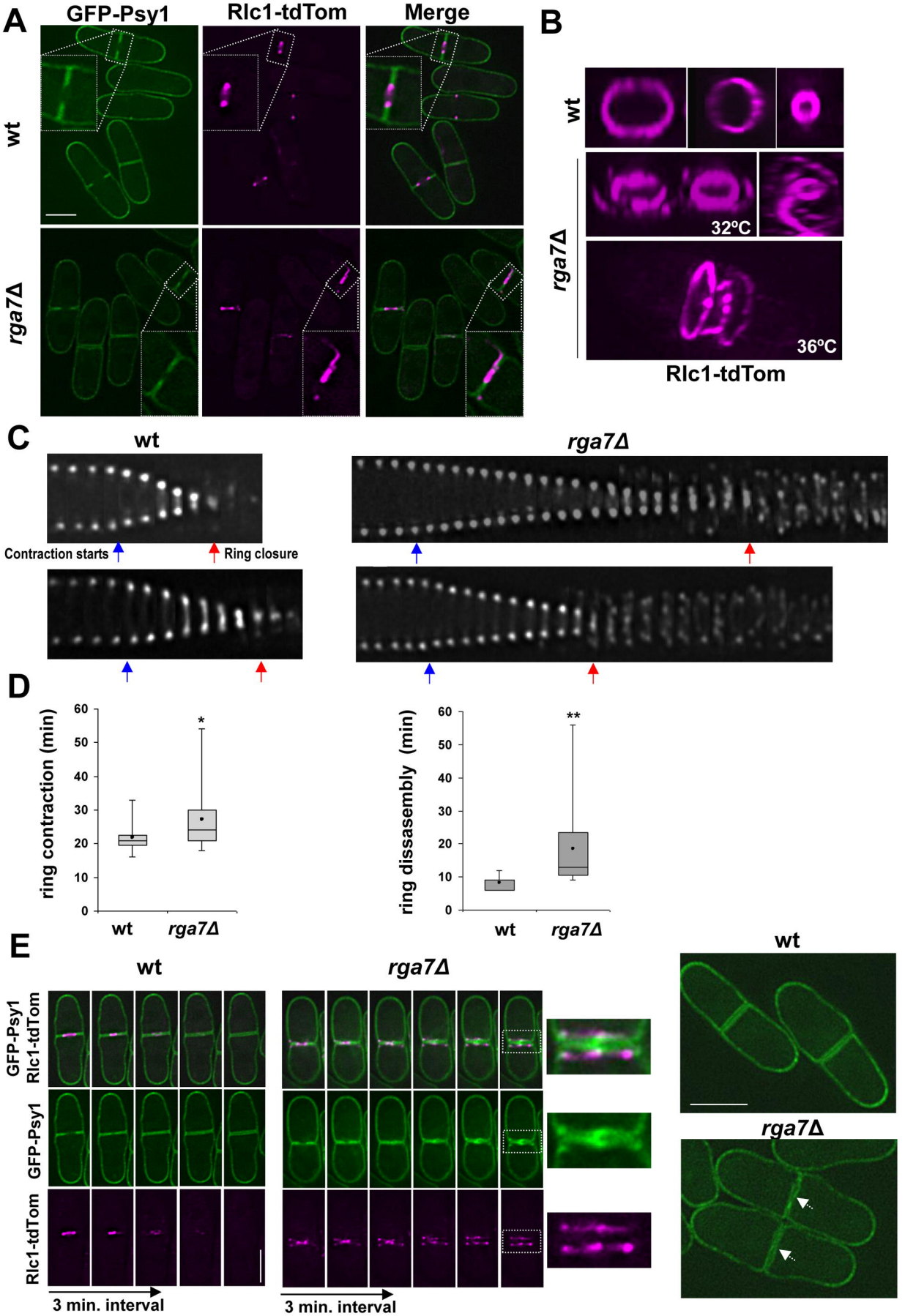

Martín-García et al., Figure 2

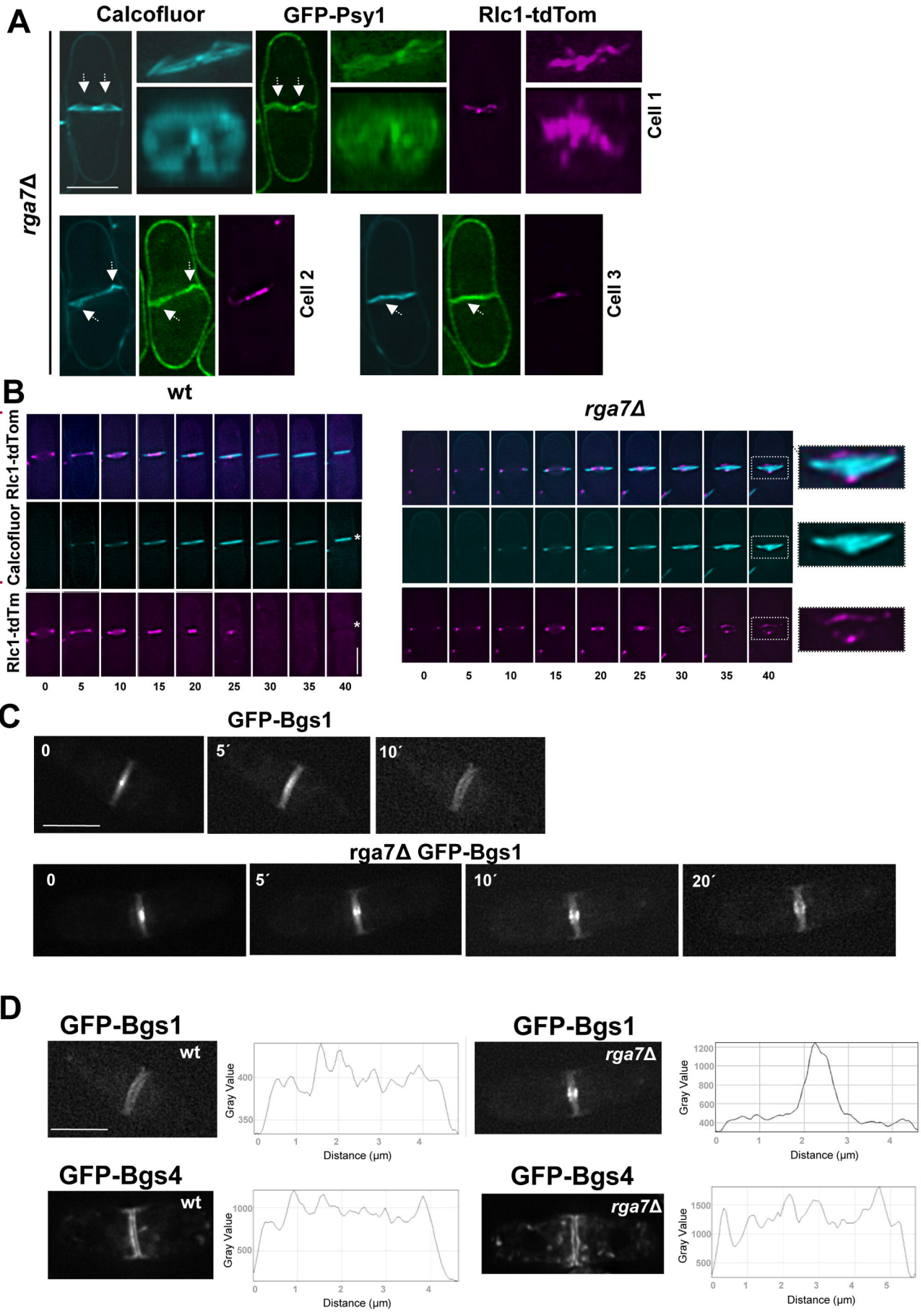

Martín-García et al., Figure 3

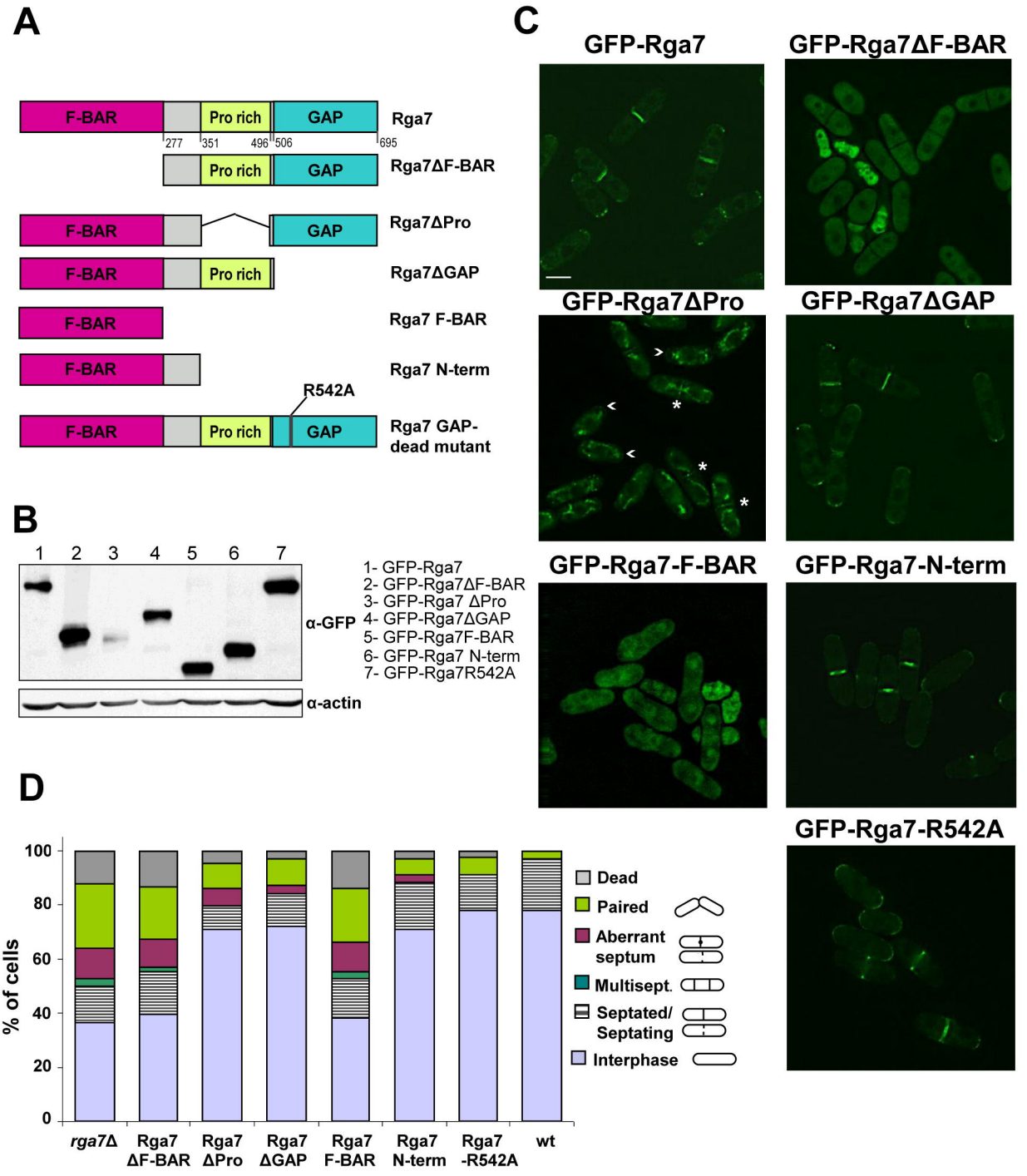

Martín-García et al., Figure 4

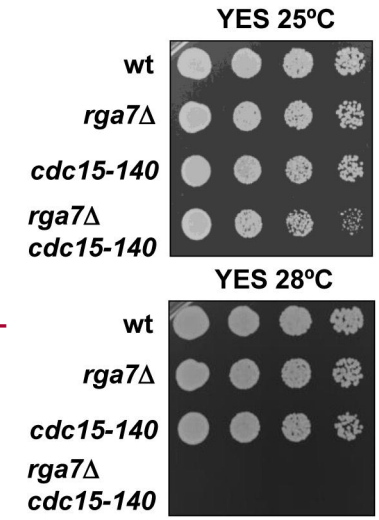

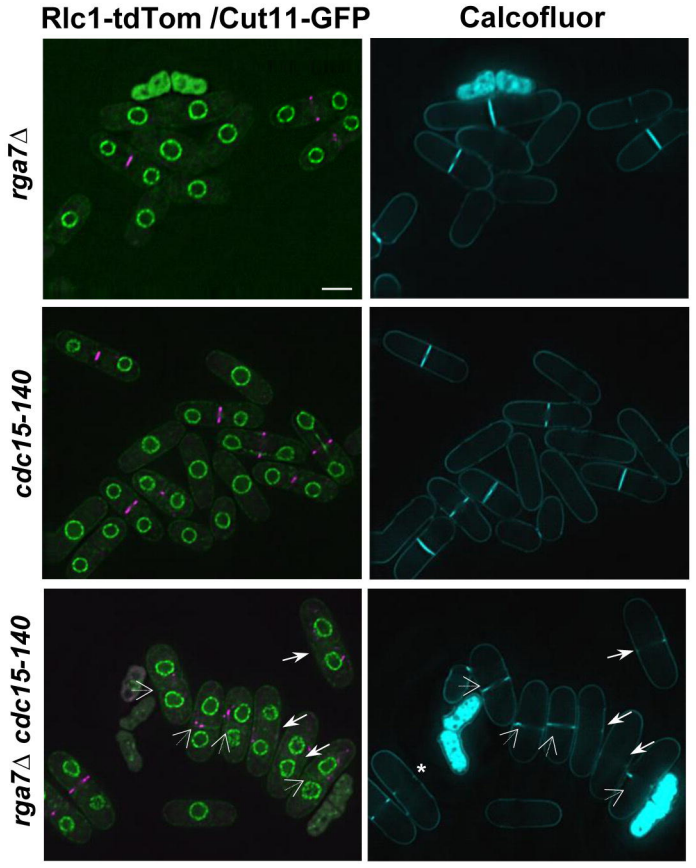

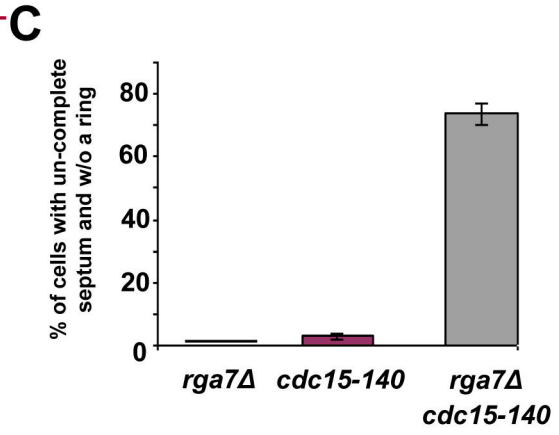

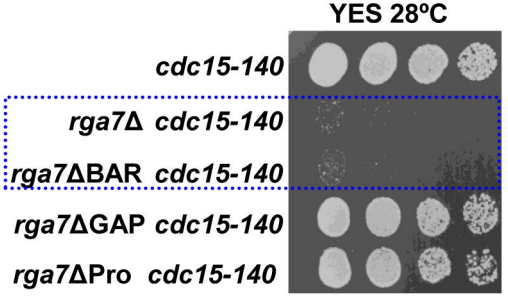

Martín-García et al., Figure 5

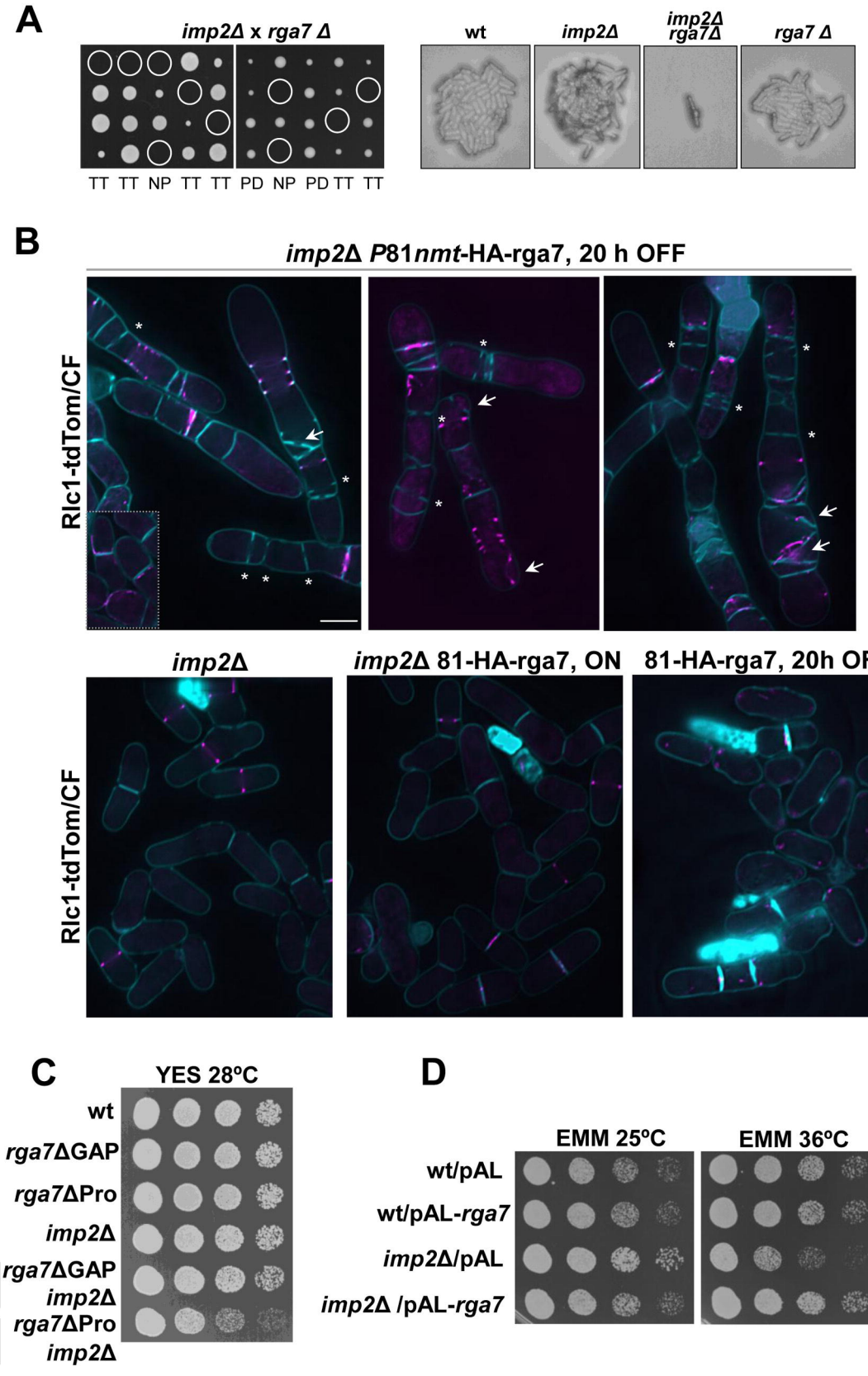

Martín-García et al., Figure 6

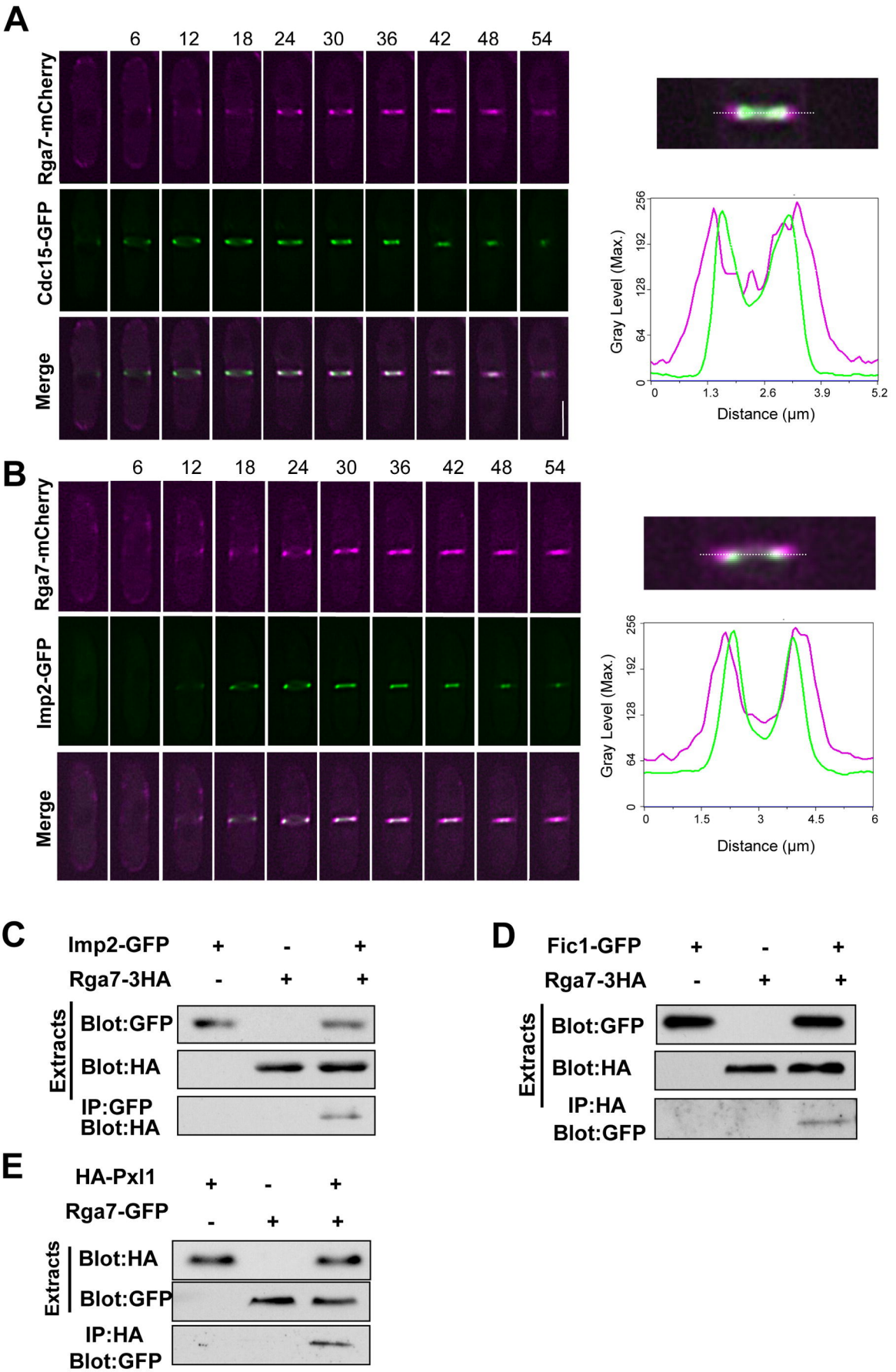

Martín-García et al., Figure 7